Applied Catalysis B: Environmental 194 (2016) 16–21

Contents lists available at ScienceDirect

Applied Catalysis B: Environmental

journal homepage: www.elsevier.com/locate/apcatb

Three dimensional CNTs aerogel/MoS_x as an electrocatalyst for hydrogen evolution reaction

Sathish Reddy*, Ran Du, Lixing Kang, Nannan Mao, Jin Zhang

Center for Nanochemistry, Beijing National Laboratory for Molecular Sciences, Key Laboratory for the Physics and Chemistry of Nanodevices, State Key Laboratory for Structural Chemistry of Unstable and Stable Species, College of Chemistry and Molecular Engineering, Peking University, Beijing 100871, China

ARTICLE INFO

Article history:
Received 10 January 2016
Received in revised form 10 March 2016
Accepted 5 April 2016
Available online 7 April 2016

Keywords:
CNTs aerogel
Molybdenum sulfides
Hydrogen evolution reaction and electrocatalysts

ABSTRACT

Preparation of electrocatalysts with high activity and low cost are essential for mass production of hydrogen. However, preparation of such catalyst are still highly challenging thus far. In this paper, we focus on preparation of a three- dimensional CNTs aerogel/MoS_x catalyst by using solvothermal process. The MoS_x material has been successfully combined with three- dimensional CNTs aerogel and creates a sufficient active site exposure as well as 3D conductive networks for fast charge transport. Due to this the catalyst exhibited high activity for HER with a small onset over potential of ~150 mV, a Tafel slope of 62 mV dec^{-1}, and an exchange current density of 6.4 mA cm^{-2}. The catalysts also show excellent stability during long-term 1000 cycles and electrolysis confirm the durability of the catalyst. The enhanced performance is attributed to synergistic effects of CNTs aerogel and MoSx, which enhance the activities for both components for HER.

1. Introduction

Hydrogen is an abundant, renewable and the cleanest fuel with zero-emission and represents one of the most promising energy carrier in future that could be used to power up electronic devices, vehicles and homes [1–4]. The most desirable source of hydrogen is water as it is abundant and contains no carbon [3]. Therefore, the efficient generation of hydrogen from water splitting by the hydrogen evolution reaction (HER) has gained more and more attention [1,5,6]. At present, platinum has been demonstrated to be a superior electrocatalyst for HER in acid media [7–9], whereas its high cost and scarcity on earth retard wide range application for HER. The same electrocatalyst is also in demand as a cathode of photoelectrochemical water splitting cells. Thus, it is desirable but challenging to find inexpensive alternatives earth–abundant material is a crucial challenge for practical large-scale hydrogen production.

Transition metal carbides, nitrides, and sulfides are known as effective candidates for replacing the Pt group metal in various catalytic processes including hydrogenation and hydrosulfurization due their similar electronic structures to that of noble metals [9,10]. It has been reported that the high HER activity for the crystalline MoS_2 structures is related to the unsaturated sulfur appearing at the crystal edges [11,12]. Additionally, the catalytic species in the amorphous MoS_x have attracted great interest as promising electrocatalyst for HER [13–15]. Moreover, aggregation of MoS_x materials also affects the dispersion and results in the decrease of activity. Thus, the modification of MoS_x materials with conductive templates or supports is proposed to be an effective way to improve the catalytic activity of the host material. By now, quite a few investigations have proved that the HER performance of MoS_x could be significantly enhanced by incorporating with graphene, carbon nanotubes (CNTs), and other mesoporous carbon to form MoS_x-based hybrid or composite [16–20]. The nanocarbons serve as templates for mediating the growth of the MoS_x and formation of specific structures, which improves the dispersion of MoS_x materials and enhances the conductivity of whole catalyst [20].

On the other hand, it was reported that electrodes based on 3D porous materials can improve the catalytical activity by increasing the electroactive surface area of the catalysts [21,22]. Combining with carbon nanostructures, 3D carbon aerogel materials not only showed high specific surface areas (SSAs), but also enhance good electrical conductivity which is beneficial for electron transfer [23,24]. Previously, we have been fabricated nitrogen-doped multi-walled carbon nanotubes (N-MWNTs or N-CNTs) aerogels by a promoter-assisted hydrothermal reaction coupling with pyrolysis [24]. Herein, MoS_x/MWNTs aerogels were synthesized by incorporating MoS_x into as-prepared CNT aerogel by a

* Corresponding author.
E-mail addresses: gnsathishreddy@gmail.com, sathish-cnc@pku.edu.cn (S. Reddy).

http://dx.doi.org/10.1016/j.apcatb.2016.04.007
0926-3373/

solvothermal process. The resultant MoS_x/MWNTs aerogel were proved to be highly active electrocatalyst for HER in 0.5 M H_2SO_4 solution with a low onset over potential (150 mV), a small Tafel slope (62 $mVdec^{-1}$), a high exchange current density (6.35 $mA\,cm^{-2}$) and good electroconductivity. Moreover, the MoS_x/MWNTs aerogel catalysts showed excellent long-term stability over 1000 cycles and further electrolysis confirmed the durability of catalyst.

2. Experimental

2.1. Materials

The multi-walled carbon nanotubes (MWNTs) were purchased from obtained from CNano Technology Company Ltd. The $(NH_4)_2MoS_4$ powder and N, N-dimethylformamide (DMF) were purchased from Sigma-Aldrich. H_2SO_4 was purchased from Aladdin Ltd. (Shanghai, China). Pt/C (20 wt% Pt on Vulcan XC-72R) and Nafion (5 wt%) were purchased from DUPONT. All chemicals were used as received without further purification. The water used throughout all experiments was purified through a Millipore system.

2.2. Preparation method

MWNTs aerogels have been synthesized according to the method reported previously [24]. The MoS_x/MWNTs aerogels were synthesized according to the a solvothermal process described elsewhere [25,26], In a typical experiment, 220 mg $(NH_4)_2MoS_4$ powder (Sigma-Aldrich) and 45 mg MWNTs aerogel were mixed and dispersed into 15 ml of N,N dimethylformamide (DMF) in a 20 ml Teflon autoclave. After that, the solution was sonicated at room temperature for approximately 10 min until homogeneous solution was achieved. Then the autoclave was sealed tightly and heated at 200 °C for 10 h under autogenous pressure without intentional control of ramping and cooling rate. After cooled down to room temperature, the product was extracted by centrifugation at 8000 rpm for 5 min. To remove the unreacted molecules and most of the DMF residuals the product was dispersed in DI water and recollected by centrifugation, this washing step was repeated for at least 5 times, the final products was MoS_x/MWNTs aerogel. The same procedure was followed for the preparation of MoS_x particles without using CNTs aerogel support.

2.3. Characterizations

The structure of the prepared MoS_x/MWNTs aerogel were studied with scanning electron microscopy (SEM Hitachi S-4800 field emission, Japan), High-resolution transmission electron microscopy (HRTEM, Tecnai F 20, FEI), X-ray diffraction (XRD) {Rigaku D/MAX 2550 diffractometer with Cu Kα radiation (λ = 1.5418 Å)}. Raman spectrometer (a Horiba HR800 Raman system A 100 objective was used to focus laser beam and to collect Raman signal). X-ray photoelectron spectroscopy (XPS) (an ESCALABMK II X-ray photoelectron spectrometer using Mg as the exciting source).

2.4. Electrochemical measurement

Electrochemical measurements are performed with a CHI660D electrochemical analyzer (CH Instruments, Inc., Shanghai). A three-electrode cell is used, including a glassy carbon electrode (GCE, geometric area = 0.07 cm^2) as the working electrode, a saturated calomel electrode (SCE) as the reference electrode, and a platinum wire as the counter electrode. The typically, 5 mg of sample & 40 μl Nafion solution (5 wt%) were dispersed in 1 ml N,N dimethylformamide (DMF) by sonicating for 30 min form a homogenous ink. Then 5 μl of the dispersion was loaded onto glassy carbon electrode with 3 mm diameter. The electrolyte (0.5 M H_2SO_4) was degassed by bubbling N_2 for at least 30 min before the electrochemical measurements. Linear sweep voltammetry (LSV) was performed in N_2 saturated aqueous solution of 0.5 M H_2SO_4 with a scan rate of 2 $mV\,s^{-1}$ in a range from 0 V to −0.8 V. Stability test was then carried out by cyclic voltammetry (CV) scanning from −0.8 to 0 vs. SCE for 1000 cycles at a scan rate of 100 $mV\,s^{-1}$. The electrochemical impedance spectroscopy (EIS) measurements were carried out from 100000 to 0.01 Hz in 0.5 M H_2SO_4 solution. In all measurements, (SCE) was used as the reference, and all the potentials reported in our work were vs. the reversible hydrogen electrode (RHE). In 0.5 M H_2SO_4, (RHE): E (RHE) = E (SCE) + (0.242 + 0.059 pH) V. All the potential data presented in the paper were corrected for iR losses.

3. Results and discussion

In this work, the MoS_x/MWNTs aerogel nanostructure synthesized by simple solvent thermal method at low temperature (200 °C) using $(NH_4)_2MoS_4$ as precursors and N,N dimethylformamide (DMF) as solvent in the presence of MWNTs aerogel. Fig. 1(A) shows MoS_x black dark films decorated on the MWNTs aerogel structures and they combine each other very closer, forming the layered structure of staggered, which is important to tightly attach the MoSx films on the surface of the MWNTs aerogel electrode. In the absence of carbon nanotube aerogel support, aggregated MoS_x particle is produced (Fig. S1) Therefore, MWNTs aerogel support would be beneficial for the deposition and formation of MoS_x nanoparticles [27], and provide a good distribution for the exposed active surface of MoS_x nanoparticles [28]. MoS_2 nanosheets are also supported on other carbon materials [29]

The HRTEM in Fig. 1(B) gives a close-up view of the MoS_x nanoparticles on the MWNTs aerogel. The layered spacing can be identified to be around ∼0.34 nm which is in good consistence with value between the graphitic planes of MWNTs and ∼0.63 nm spacing values may be due to between the MoS_x planes of MoS_x nanoparticles is not clear probably due to semi-crystalline nature of the MoS_x nanoparticles. Each MoS_x nanoparticles is composed of diffused rings and indicate semi-crystalline nature is confirmed by selected-area electron diffraction (SAED) pattern as shown in Fig. S2. After annealing at 800 °C under Ar protecting environment of MoS_x/MWNTs aerogel sample it's changed to MoS_2 black dark layered films wedded aspect on the MWNTs aerogel structures (MoS_2/MWNTs aerogel) as shown in Fig. 1(C), which might be due to MWNTs aerogel structures supports to form MoS_x nanoparticle and after thermal annealing the MoS_x nanoparticle changed to crystalline MoS_2 layered films on MWNTs aerogel structures [25]. Similarly, reported that C@MoS_2 nanoboxes are further annealed at 700 °C in H_2 for 2 h changed to highly crystalline layered MoS_2 nanosheets support on other carbon materials [29]. The HRTEM in Fig. 1(D) gives a close-up view of the MoS_2 nanoparticles on the MWNTs aerogel. The layered spacing can be identified to be around ∼0.34 nm which are in good consistence with value between the graphitic planes of MWNTs and ∼0.63 nm spacing values due to between the MoS_2 planes of MoS_2 nanoparticles is clearly indicated that crystalline nature of the MoS_2 nanoparticles. HRTEM also image showing Moiré fringes due to the overlap of multiple MoS_2 (5–6) layers; which is good consistent with literature reported value of MoS_2 [25,29,30].

X-ray photoelectron spectroscopy (XPS) was used to investigate the chemical states of Mo and S in the MoS_x/MWNTs aerogel. Fig. 2 displays the XPS characterization of the samples before and

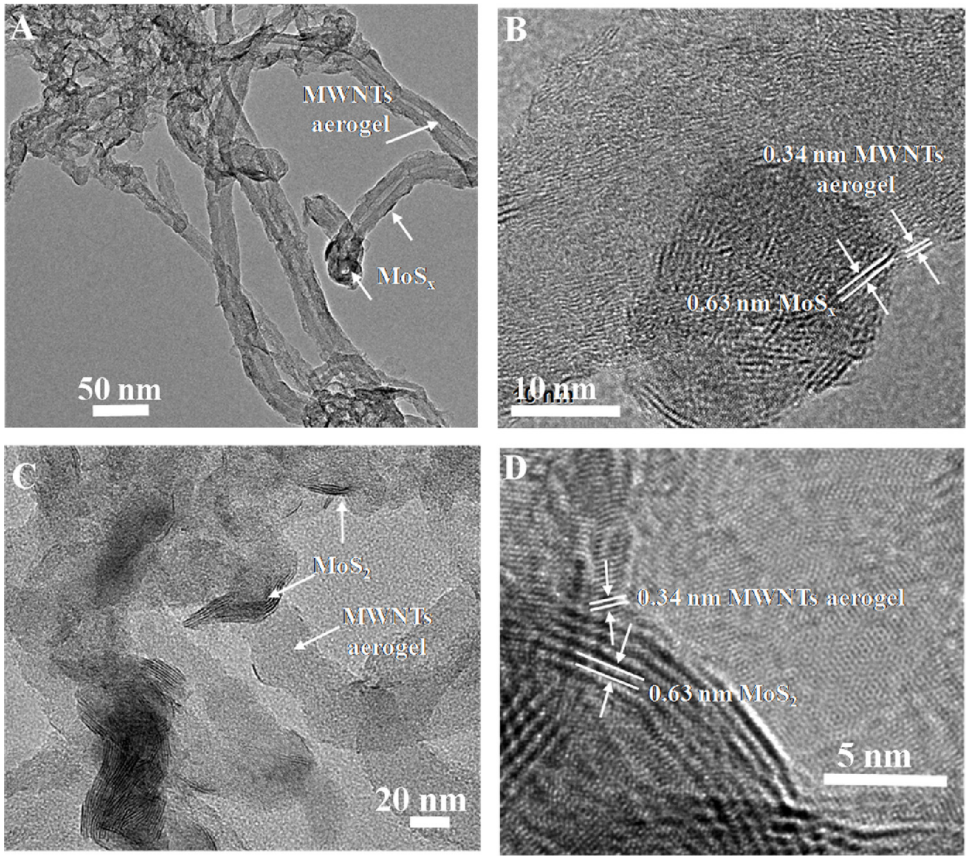

Fig. 1. TEM (A) and HRTEM (B) image of MoS_x/CNTs aerogel, TEM image of MoS_2/CNTs aerogel (C) and (D) HRTEM image of MoS_2/CNTs aerogel.

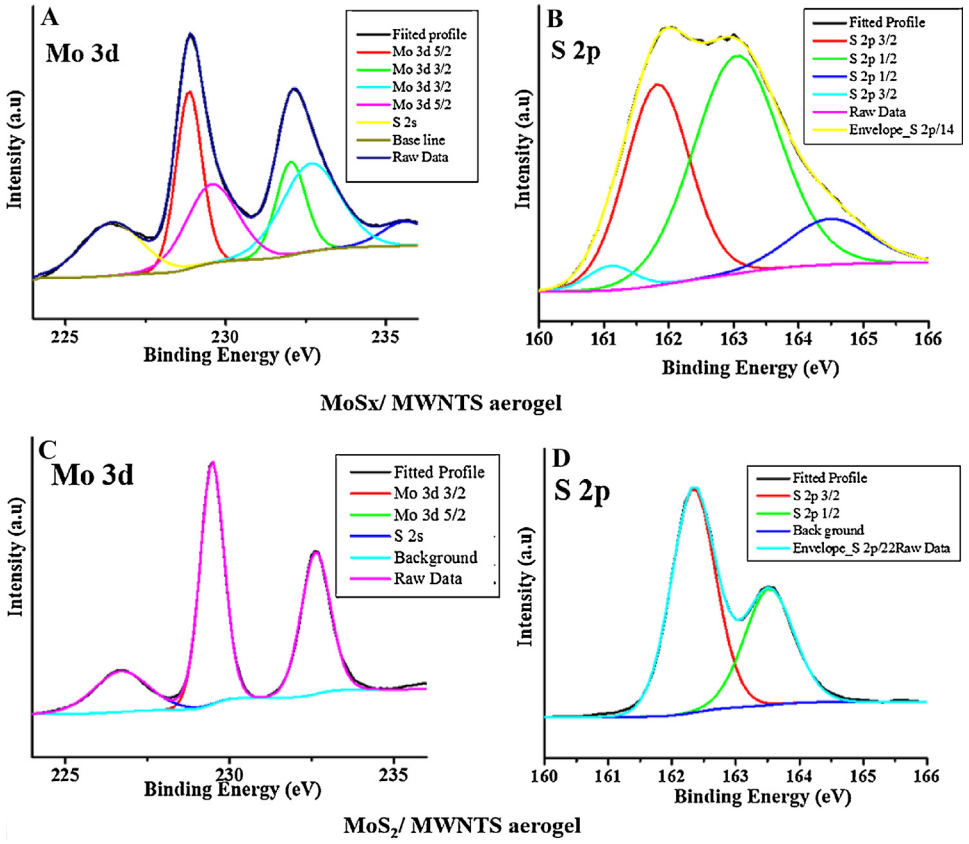

Fig. 2. XPS of MoS_x/MWNTS aerogel before annealing at 800 °C (A &B) and MoS_x/MWNTS aerogel after annealing at 800 °C (C &D).

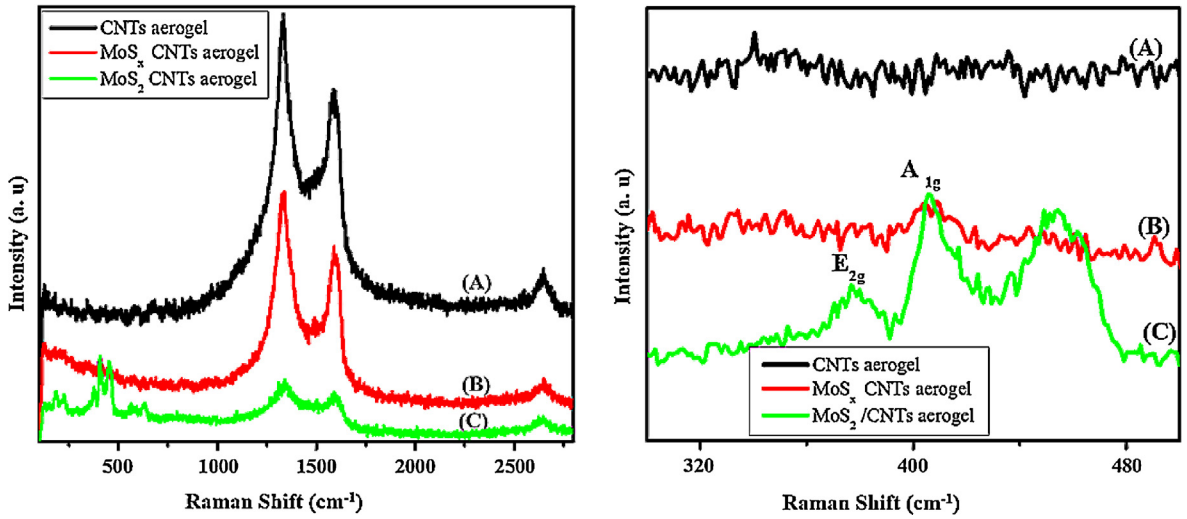

Fig. 3. Raman Spectra of MWNTS aerogel (A), MoS_x/MWNTS aerogel (B) and MoS_2/MWNTS aerogel C) (after annealing at 800 °C).

after thermal annealing at 800 °C under Ar protecting environment. The high-resolved XPS spectra shows the binding energies of Mo 3d 3/2, Mo 3d 5/2, S 2p 1/2 and S 2p 3/2 peaks in the thermal annealed MoS_x/MWNTs aerogel are located at 232.4, 229.2, 163.3 and 162.1 eV, respectively, indicating that Mo^{+4} existed in the annealed MoS_x/MWNTs [25,31]. For the as prepared MoS_x/MWNTs aerogel two broaden peaks centered at 232.5 and 228.9 eV, in addition to the XPS peaks for MoS_2 structure, other sets of peaks are also observed. The higher energy shift of Mo 3d 3/2 and 3d 5/2 doublet are associated with higher valence states. The observation of Mo 3d 3/2 and Mo 3d 5/2 peaks at 233.6 and 230.5 eV with separation energies close to 3.1 eV can be attributed to the presence of Mo^{5+} ions [25,32,33]. For the non-annealed MoS_x/MWNTs the S 2p spectra can be interpreted in terms of two doublets, with S 2p3/2 binding energies of 161.7 and 163.2 eV. Compared to the thermal annealed samples, the additional S 2p1/2 and 2p3/2 energies located at 164.3 and 163.2 eV can be assigned to the binding energies of apical S^{2-} or bridging disulfide S_2^{2-} ligands.

Fig. 3(A)–(C) compare the Raman spectra taken from the as obtained MWNTs aerogel, MoS_x/MWNTs aerogel samples and thermal treated MoS_2/MWNTs aerogel. The Raman Peaks at around 1347 and 1576 cm^{-1} belong to MWNTs. The 2D-band of MWNTs aerogel locates at 2686 cm^{-1}. The Raman Peaks of MoS_2 appear at 376 and 402 cm^{-1}. It was also found that the Raman signature of MoS_2 dramatically increased after thermal annealing, which suggests the formation of highly crystallized MoS_2 layers.

Further confirmation of the MWNTs aerogel, MoS_x/MWNTs aerogel and MoS_2/MWNTs aerogel was examined by XRD, as shown in Fig. 4(A)–(C). XRD patterns of hexagonal MoS_2 supported on the MWNTs aerogel are shown in Fig. 4(C), which are consistent with their reference hexagonal (JCPDS No.17-0744). Fig. 4(B) shows broad peaks in between $2\theta = 35°$ to 70 which indicate that semicrystalline nature of MoS_x nanoparticles on MWNTs aerogel, Fig. 4(A) shows with the diffraction angle at $2\theta = 26.24°$ corresponds to the characteristic peak of MWCNTs aerogel.

The HER properties of the MoS_x/MWNTs aerogel, MoS_x particles, MoS_2/MWNTs aerogel, MWNTs aerogel and GCE were then investigated in 0.5 M H_2SO_4 solutions using a typical three-electrode system. For comparison study, Pt/C catalyst was also examined. Fig. 5A shows the polarization curves with a sweep rate of 2 mV s^{-1}. Pt/C catalyst exhibits expected HER activity with a nearly zero over potential, whereas GCE exhibit poor HER activity. In contrast, MoSx/MWNTs aerogel (a) exhibit small onset over potential of −150 mV, which is much smaller than that of other

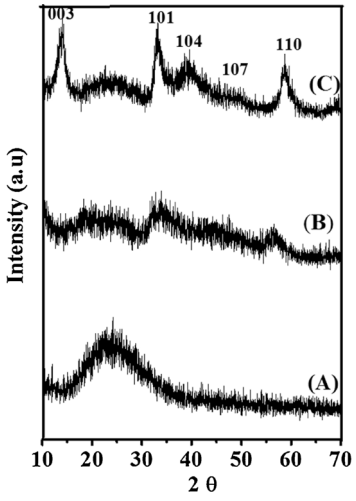

Fig. 4. XRD pattern of MWNTS aerogel (A), MoS_x/MWNTS aerogel (B) and (after annealing at 800 °C) MoS_2/MWNTS aerogel (C).

MoS_x, MoS_2/MWNTs aerogel, MWNTs aerogel and GCE (−190 mV, −210 mV, −320 mV, and −350 mV).

Fig. 5B shows Tafel plots [over potential vs log (current density)] MoSx/MWNTs aerogel and 20%Pt/C. The 20% Pt/C exhibits a Tafel slope of 32 mV/decade and MoSx/MWNTs aerogel exhibits a Tafel slope of 62 mV/decade, which is much smaller than that of other MoS_x, MoS_2/MWNTs aerogel and MWNTs aerogel (71 mV/decade, 135 mV/decade and110 mV/decade). These results suggest MoSx/MWNTs aerogel catalysts their hydrogen evolution occurs through various reaction pathways proceed via a Volmer-Heyrovsky mechanism [34–36].

The exchange current density (j_0) is also given, which can be obtained from Tafel plots by using extrapolation methods (see Fig. S3for details). The j_0 for MoSx/MWNTs aerogel is determined as 6.4 mA cm^{-2}, which is relatively higher exchange current value for HER catalysts than those recently reported elsewhere [13,15,37–41] (Table1). MoSx/MWNTs aerogel catalysts ought to achieve good electroconductivity, and we thus performed electrochemical impedance spectroscopy (EIS) measurements. Fig. 5C shows Nyquist plot with an equivalent circuit of MoS_x/MWNTs aerogel ($R_{ct} = 75.91\ \Omega$), MoS_x particles ($R_{ct} = 210.10\ \Omega$), & MoS_2/MWNTs aerogel ($R_{ct} = 350.21\ \Omega$). The charge-transfer resistance R_{ct} is related the electrocatalytic kinet-

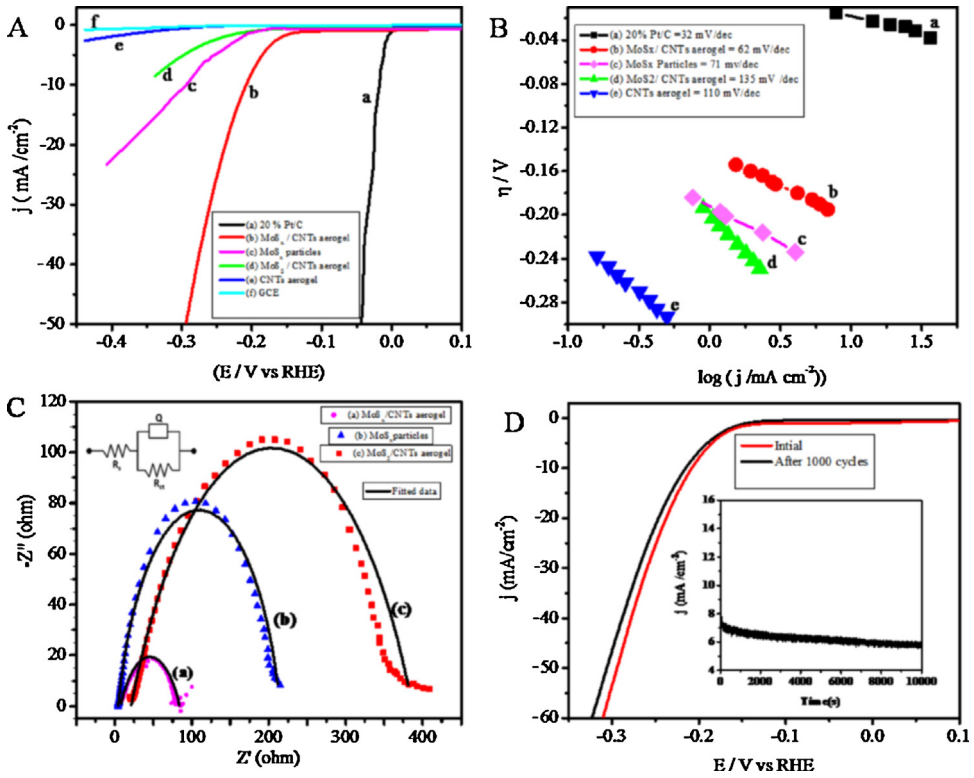

Fig.5. (A) Polarization Curves, (a) 20% Pt/C, (b) MoS_x/CNTs aerogel, (c) MoS_x particles, (d) MoS_2/CNTs aerogel, (e) CNTs aerogel, and (f) GCE catalysts with a scan rate of 2 mV s^{-1} in 0.5 M H_2SO_4,(B) Tafel plot, (C) Nyquist plot with an equivalent circuit of the (a) MoS_x/CNTs aerogel, (b) MoS_x particles, (c) MoS_2/CNTs aerogel, (Dotted line: measured data and Solid line: fitted data) and (D) Stability test display negligible current loss even after 1000CV cycles and also inset shows time dependence of current density under static overpotential of 180 mV.

Table 1
Comparison of HER performance with other non-noble metal electrocatalysts.

Materials	Overpotentials (mV)	Tafel Slope (mV/dec)	Exchange current ($mAcm^{-2}$)	Reference
MoS_x		50.5	1.5	[13]
PPy/MoS_x		29	0.56	[15]
MoS_x-G	130	43		[37]
$[Mo_3S_{13}]_2$ cluster	100–120	40		[38]
MoS_x/graphene/Ni foam	130	42.8		[39]
Molybdenum Sulfide/N-Doped grapheme hydrogel		105		[40]
Amorphous molybdenum sulfide films	40	40	0.13	[41]
MoS_x/MWNTs aerogel	150	62	6.353	Present work

ics and a lower value corresponds to a faster reaction rate [41–43], R_u is uncompensated resistance and constant phase element (Q) is used instead of capacitor to account for surface heterogeneity. The impedance of a CPE is $Z(Q) = (1/y_o)/ (j.\ \omega)^n$,where $y_o$is a constant with dimension Fs^{n-1}, $j = (-1)^{1/2}$, $\omega = 2\pi f$ and n is the constant between 0 and 1, n=1 represents ideal capacitor [41,44]. The R_{ct} value of MoS_x/MWNTs aerogel is smaller than that of MoS_x & MoS_2/MWNTs aerogel composite. Therefore, MoS_x/MWNTs aerogel shows the best HER activity, which is consistent with result obtained from polarization measurement (Fig. 5A) and also for details comparison of impedance parameter with HER results were listed in Table S1. The low charge-transfer resistance is beneficial to achieve highly efficient charge transport, owing to the synergistic effect from the MoS_x and the excellent electrical coupling to the conductive MWNTs aerogel. We also performed the durability test of the MoS_x/MWNTs aerogel catalysts utilizing cyclic voltammetry (CV) measurements for scanning 1000 cycles in 0.5 M H_2SO_4. The observation of negligible current loss (Fig. 5D) indicates that the MoS_x/MWNTs aerogel catalysts have good electrochemical stability in acidic electrolyte. Further, the practical operation of the catalyst is examined by electrolysis at fixed potential over

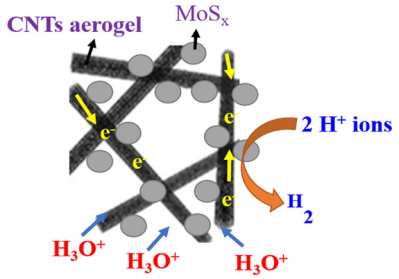

Scheme 1. Schematic diagram showing the mechanism of hydrogen evolution reaction solution at surface of MoS_x/MWNTS aerogel.

long period. The current density exhibits only degradation after a long period of 10,000 s (Fig. 5D inset), which might be caused by the consumption of H^+ or the remaining of H_2 on the surface of the electrode that hindered the reaction [28]. All these results demonstrate the MoS_x/MWNTs aerogel are indeed a highly efficient HER electrocatalyst. The MoS_x/MWNTs aerogel catalysts exhibit high activity for HER. This probable may be due to structure is pro-

vided by the MWNT aerogels, and the MWNT aerogels supports suppress the aggregation of MoS_x nanoparticles which enhanced more exposed active surface, rapid diffusion of ions and electrons on the MoS_x/MWNTs aerogel surface schematically shown in Scheme1 which demonstrate low over voltage, low Tafel slope, high exchange current density (j_0) and good stability in acidic solution for hydrogen evolution reaction.

4. Conclusion

In summary, MoS_x/MWNTs aerogel have been successfully synthesized via a solvothermal process. We further demonstrate the use of such MoS_x/MWNTs aerogels as a novel HER electrocatalyst with high efficiency. The catalyst shows onset overpotential of −150 mV and Tafel slope 62 mV/dec in 0.5 M H_2SO_4. The MWNTs aerogel provides a large surface area for the active MoS_x to contact readily with liquid electrolytes and serves as supporting materials to stabilize MoSx nanoparticles .Therefore, the MoSx/MWNTs aerogel electrocatalyst exhibits an ehnaced activity, stablity and durablity for HER..

Acknowledgements

This work was supported by the NSFC (Grants 21233001, 21129001, 51272006 and 51121091) and the MOST (Grant 2011CB932601).

Appendix A. Supplementary data

Supplementary data associated with this article can be found, in the online version, at http://dx.doi.org/10.1016/j.apcatb.2016.04.007.

References

[1] M.S. Dresselhaus, I.L. Thomas, Nature 414 (2001) 332–337.
[2] N.S. Lewis, D.G. Nocera, Powering the planet: chemical challenges in solar energy utilization, Proc. Natl. Acad. Sci. U.S.A. 103 (2006) 15729.
[3] J.A. Turner, Sustainable hydrogen production, Science 304 (2004) 1972–1974.
[4] J. Nowotny, C.C. Sorrell, L.R. Sheppard, T. Bak, Int. J. Hydrogen Energy 30 (2005) 521–544.
[5] A.J. Bard, M.A. Fox, Acc. Chem. Res. 28 (1995) 141–145.
[6] M.G. Walter, E.L. Warren, J.R. McKone, S.W. Boettcher, Q. Mi, E.A. Santori, N.S. Lewis, Chem. Rev. 110 (2010) 6446–6473.
[7] Y. Hara, N. Minami, H. Matsumoto, H. Itagaki, Appl. Catal. A: General 332 (2007) 289–296.
[8] M. Wu, P. Shen, Z. Wei, S. Song, M. Nie, J. Power Sources 166 (2007) 310–316.
[9] E. Furimsky, Appl. Catal. A 240 (2003) 1–28.
[10] J.G. Chen, Chem. Rev. 96 (1996) 1477–1498.
[11] J. Greeley, T. Jaramillo, J. Bonde, I. Chorkendorff, J. Nørskov, Nat. Mater. 5 (2006) 909–913.
[12] T.F. Jaramillo, K.P. Jorgensen, J. Bonde, J.H. Nielsen, S. Horch, I. Chorkendorff, Science 317 (2007) 100–102.
[13] C.L. Hsu, Y.H. Chang, T.Y. Chen, C.C. Tseng, K.H. Wei, L.J. Li, Int. J. Hydrogen Energy 39 (2014) 4788–4793.
[14] B. Seger, A.B. Laursen, P.C.K. Vesborg, T. Pedersen, O. Hansen, S. Dahl, I. Chorkendorff, Angew. Chem. Int. Ed. 51 (2012) 9128–9131.
[15] T. Wang, J. Zhuo, K. Du, B. Chen, Z. Zhu, Y. Shao, M. Li, Adv. Mater. 26 (2014) 3761–3766.
[16] Y. Yan, X. Ge, Z. Liu, J.Y. Wang, J.M. Lee, X. Wang, Nanoscale 5 (2013) 7768–7771.
[17] T.W. Lin, C.J. Liu, J.Y. Lin, Appl. Catal. B 75 (2013) 134–135.
[18] X. Bian, J. Zhu, L. Liao, M.D. Scanlon, P. Ge, C. Ji, H.H. Girault, B. Liu, Electrochem. Commun. 22 (2012) 128–132.
[19] D.J. Li, U.N. Maiti, J. Lim, D.S. Choi, W.J. Lee, Y. Oh, G.Y. Lee, S.O. Kim, Nano Lett. 14 (2014) 1228–1233.
[20] Y. Yan, B.Y. Xia, Z. Xu, X. Wang, ACS Catal. 4 (2014) 1693–1705.
[21] S. Chen, J. Duan, M. Jaroniec, S.Z. Qiao, Angew. Chem. Int. Ed. 52 (2013) 13567–13570.
[22] S.H. Lim, H.I. Elim, X.Y. Gao, A.T.S. Wee, W. Ji, J.Y. Lee, Phys. Rev. B 73 (2006) 045402.
[23] L. Chen, C. Xu, R. Du, Y. Mao, C. Xue, L. Chen, L. Qu, J. Zhang, T. Yi, J. Mater. Chem. A 3 (2015) 5617–5627.
[24] R. Du, N. Zhang, J. Zhu, Y. Wang, C. Xu, Y. Hu, N. Mao, H. Xu, W. Duan, L. Zhuang, L. Qu, Y. Hou, J. Zhang, Small 11 (2015) 3903–3908.
[25] Y. Shi, Y. Wang, J.I. Wong, A.Y.S. Tan, C.L. Hsu, L.J. Li, Y.C. Lu, H.Y. Yang, Sci. Rep. 3 (2013) 1–7.
[26] Y. Yan, B. Xia, X. Qi, H. Wang, R. Xu, J.Y. Wang, H. Zhang, X. Wang, Chem. Commun. 49 (2013) 4884–4886.
[27] B.Y. Xia, Y. Yan, X. Wang, X.W. (David) Lou, Mater. Horiz. 1 (2014) 379–399.
[28] J. Xie, H. Zhang, S. Li, R. Wang, X. Sun, M. Zhou, J. Zhou, X.W. (David) Lou, Y. Xie, Adv. Mater. 25 (2013) 5807–5813.
[29] X.Y. Yu, H. Hu, X.W. Lou, Angew. Chem. Int. Ed. 54 (2015) 7395–7398.
[30] D.J. Late, Y.K. Huang, B. Liu, J. Acharya, S.N. Shirodkar, J. Luo, A. Yan, D. Charles, U.V. Waghmare, V.P. Dravid, C.N.R. Rao, ACS Nano 7 (2013) 4879–4891.
[31] V.O. Koroteev, L.G. Bulusheva, I.P. Asanov, E.V. Shlyakhova, D.V. Vyalikh, A.V. Okotrub, J. Phys. Chem. C 115 (2011) 21199–21204.
[32] M.A. Baker, R. Gilmore, C. Lenardi, W. Gissler, Appl. Surf. Sci. 150 (1999) 255–262.
[33] H.W. Wang, P. Skeldon, G.E. Thompson, Surf. Coat. Technol. 91 (1997) 200–207.
[34] A. Lasia, Handbook of Fuel Cells, in: W. Vielstich, H.A. Gasteiger, A. Lamm, H. Yokokawa (Eds.), Wiley, 2010.
[35] Y. Zheng, Y. Jiao, M. Jaroniec, S.Z. Qiao, Angew. Chem. Int. Ed. 54 (2015) 52–65.
[36] J. Thomas, Kinetics of electrolytic hydrogen evolution and the adsorption of hydrogen by metals, Trans. Faraday Soc. 57 (1961) 1603.
[37] Z. Pu, Q. Liu, A.M. Asiri, A.Y. Obaid, X. Sun, J. Power Sources 263 (2014) 181–185.
[38] J. Kibsgaard, T.F. Jaramillo, F. Besenbacher, Nat. Chem. 6 (2014) 248–253.
[39] Y.H. Chang, C.T. Lin, T.Y. Chen, C.L. Hsu, Y.H. Lee, W. Zhang, K.H. Wei, L.J. Li, Adv. Mater. 25 (2013) 756–760.
[40] S. Chen, J. Duan, Y. Tang, B. Jin, S.Z. Qiao, Nano Energy 11 (2015) 11–18.
[41] Y. Yan, X.M. Ge, Z.L. Liu, J.Y. Wang, J.M. Lee, X. Wang, Nanoscale 5 (2013) 7768–7771.
[42] D. Merki, H. Vrubel, L. Rovelli, S. Fierro, X.L. Hu, Chem. Sci. 3 (2012) 2515–2525.
[43] S. Peng, L. Li, X. Han, W. Sun, M. Srinivasan, S.G. Mhaisalkar, F. Cheng, Q. Yan, J. Chen, S. Ramakrishna, Angew. Chem. Int. Ed. 53 (2014) 12594–12599.
[44] A.M.A. Alsamuraee, H.I. Jaafer, H.A. Ameen, A.Q. Abdullah, Am. J. Sci. Ind. Res. 2 (2011) 761–768.